Chiral organosilica particles and their use as inducers of conformational deracemization of liquid crystal phases

Orit Cohen^a, Andrew J. Ferris^b, Raymond Adkins^b, Robert P. Lemieux^c, David Avnir*a,d, Dmitri Gelman^a and Charles Rosenblatt*,b,a

Abstract

Chiral organosilica particles of size ~200 nm were synthesized from an enantio-pure multi-armed chiral D-maltose organosilane precursor in the absence of co-condensation with an achiral monomer. *Two* distinct experiments were performed to demonstrate the particles' ability to induce conformational deracemization of a host liquid crystal. The first involves an electric field-induced tilt of the liquid crystal director in the deracemized smectic-A phase. The other involves domain wall curvature separating left-and right-handed liquid crystal helical pitch domains imposed by the cells' substrates. The results demonstrate unequivocally that enantio-pure organosilica nanoparticles can be synthesized and can induce chirality in a host.

a. Institute of Chemistry, the Hebrew University of Jerusalem, Jerusalem, 9190401;

b. Department of Physics, Case Western Reserve University, Cleveland, Ohio 44106, USA;

c. Department of Chemistry, University of Waterloo, Waterloo, Ontario, Canada N2L 3G1.

d. The H. M. Kruger Center for Nanoscience and Nanotechnology, the Hebrew University of Jerusalem, Jerusalem, 9190402, Israel

^{*}Authors for correspondence: david.avnir@mail.huji.ac.il and rosenblatt@case.edu

Introduction

We focus on two related aspects of chiral materials: The first synthesis of enantio-pure chiral sub-micron particles which are derived solely from a chiral trialkoxyorganosilane; and their use as conformational deracemization inducers of liquid crystal (LC) phases, detected by observing the electroclinic effect (ECE) and by employing the Raynes' geometry experiment, both of which are explained below. Our central result is that these enantio-pure organosilica particles deracemize the surrounding liquid crystal, resulting in both electro- and mechano-optical behavior that can occur only in the presence of (induced) chirality in the liquid crystal.

Chiral functionality traditionally has been incorporated in silica particles, films and bulk powders by a number of approaches: Adsorption of chiral species on the silica surface; entrapment of chiral species within silica matrices^{1,2}; chiral imprinting of silicas³⁻⁶; surface derivatization, usually by silylation of the silanols with chiral agents⁶⁻¹⁰; co-condensation of the chiral organosilanes with Si(OR)4 [Refs. 11-13]; and pure polycondensation of solely chiral organotrialkoxysilanes^{8,14-18}, which is at the focus of this report. Chiral oxide particles — particularly silicas — have been employed extensively in chromatographic enantio-separations^{12,19-23} and in enantioselective catalysis^{10,11,24-29}. It comes as a surprise that chiral sub-micron particles based on enantio-pure polycondensation of chiral organotrialkoxysilanes — reported here — is unknown. The closest relevant study we could find is the work of Hao and al³⁰ who reported the polycondensation of (1R,2S,4R,5S)-exo,exo-2,5-bis(trimethoxysilyl)-bicycle-[2,2,1]heptane into large (tens of microns) chiral porous particles.

Our second focus is the use of liquid crystals to probe the ability of our chiral particles to induce deracemization in the otherwise conformationally racemic environment of the LCs. The idea is the following³¹: Molecules that display LC properties — for example, those used in this report and shown in Figs. 1a and 1b, are usually characterized by high conformational flexibility and low thermal interconversion barriers, both of the aliphatic side chains and of the rotational angle between the two aromatic parts. Classically the LCs shown in Figs. 1a,b are labelled "achiral", but in fact this achirality

reflects the net contributions of many conformers, the majority of which are devoid of any mirror symmetry (or any other improper symmetry). In the absence of any external chiral interaction, statistically there is no enantiomeric excess for any of the chiral conformers of an LC chiral phase, that is, the equilibrium state of the LC is racemic. This changes if external chiral interactions exist, for example, by doping the LC with an enantio-pure chiral species^{32,33}. In that case, the dopant will enter different diastereomeric interactions with the enantiomers of the flexible molecules, and the LC will display an excess in enantiomeric populations of a chiral phase: "deracemization", *i.e.*, "chiral induction" occurs^{32,33}. If the external chiral entity is a surface (the flat surface of a slide, or the curved surface of a particle or a pore), then the resulting enantiomer excess propagates away from the surface from one LC molecule to the next over some characteristic distance

Figure 1 (a) The liquid crystal pentylcyanobiphenyl (5CB). (b) The liquid crystal 9OO4. (c) The chiral octasilylated D-maltose precursor.

of order a few to tens of nanometers^{32,34,35}. This was demonstrated for a chiral periodic mesoporous organosilica matrix obtained by co-condensation with 15 w/w% of an (S)-binaphthyl monomer^{36,37}.

Specifically, the precursor we used for the polycondensation into the chiral particles, was the unique octa-silylaled D-maltose shown in Fig. 1c (see Supplementary Information for its synthesis), tailored for high branching of the resulting material, and which eliminates the common need for Si(OR)₄ as a co-precursor.

Two very different types of LC-related chiral induction analyses are used in this report with these particles, providing mutual confirmation of the particles' ability to induce chirality in the LC. The first is the electroclinic effect (ECE), an electromechanical effect probed by polarized light. Here the director orientation of a chiral liquid crystal in a smectic-A (Sm-A) phase tilts by an angle θ with respect to the normal to the smectic layer plane, where θ is proportional to an applied electric field E [Ref. 38]. This tilt increases with the enantiomeric excess because the applied electric field biases the molecular rotation about its long axis, resulting in an average tilt $\theta_{\rm eff}$ of the molecule in a plane perpendicular to \vec{E} . The local sense of tilt can be right or left handed, and thus for an achiral or racemic LC the average value of $\theta_{eff} = 0$. However, a certain handedness of tilt about the electric field axis is preferred when the overall mirror symmetry of the LC is broken, and θ_{eff} increases with the chiral strength. The ECE technique does not respond to achiral impurities — molecular or particulate — and its sign does not necessarily correspond to the sense of director twist of the bulk chiral nematic phase. However, it is exquisitely sensitive to the magnitude of enantiomeric excess, and can be used commercially for detection of optical impurities in pharmaceuticals³⁹. θ_{eff} can be measured by judicious choice of optical geometry, with the polarized laser intensity through the sample and analyzer being proportional to θ_{eff} . Previously we used the ECE, which is detected optically by measuring the transmitted polarized light intensity (which is proportional to θ_{eff} for an appropriately chosen experimental geometry⁴⁰) as a function of E to demonstrate chiral induction of LCs within chirally derivatized the pores 36,37 .

The second method exploited here is the helical twist of the director in the nematic phase, the so-called "Raynes' Geometry Experiment" Here a cell is fabricated in which the substrates are treated for planar orientation of the LC, with the substrates' "easy axes" for orientation mutually rotated by 90°. This forces the LC orientation to undergo a 90° rotation from one substrate to the other in order to satisfy the imposed boundary conditions. For an achiral liquid crystal, the left- or right-handed rotations are energetically equivalent, and therefore domains of both senses of twist nucleate on cooling the LC from the isotropic into the nematic phase, with clearly visible straight walls separating the domains. But if the

LC is chiral, the sense of rotation that corresponds to the natural helix of the chiral nematic is energetically favored. As a result, this favorable chiral domain grows at the expense of the less favorable domain, resulting in curved walls that bow into the "minority handedness" region, *i.e.*, into the domain in which the LC's sense of rotation is opposite to that of its natural helicity. Systematic wall curvature is a necessary consequence liquid crystalline chirality, and does not occur in the absence of chirality⁴¹. The domain boundaries can be observed by means of polarized optical microscopy, with the polarizer orientations being adjusted to maximize the contrast between the walls and the oppositely helical domains that they separate. Appropriate image software can be employed to identify points along the domain walls, which in turn can be fitted numerically to obtain the curvature. The deduced curvature is a measure of the magnitude of the chirality, with straight walls (zero curvature) corresponding to an achiral or racemic LC. The Raynes experiment is not sensitive, however, cannot indicate the net handedness if this is not known a priori.

Experimental details

Chemicals:

D-maltose monohydrate was purchased from BDH, 3-triethoxysilylpropyl isocyanate from Gelest, and Pluronic P123 from Aldrich. The commercial polyamic acid PI-2555, which is commonly used to treat substrates for planar liquid crystal alignment, was obtained from Dupont. The liquid crystal pentylcyanobiphenyl (5CB, Fig. 1a) was purchased from Merck and used as received. This LC has the following phase sequence Crystal – 22 °C – Nematic – 35 °C – Isotropic. The liquid crystal 9OO4 (Fig. 1b) has the following phase sequence: Crystal – 35° –Smectic-B – 50° –Smectic-C – 62° – Smectic-A – 73° – Nematic – 87° – Isotropic.

Preparation of the chiral particles:

The organosilane monomer, Fig. 1c, was prepared from D-maltose and 3-triethoxysilylpropyl isocyanate, as described in the Supplementary Information. For the particles preparation, 1.99 g Pluronic P123, 6.2 g KCl, 8.76 g 2M HCl solution and 71.96 gr of water were stirred and heated to 40°C in a

Pyrex pressure tube. Then, 1.5 ml of the maltose precursor in 3.0 mL of ethanol was added to the clear solution and the mixture was stirred at 40 °C over-night. The mixture was then heated to 100 °C for 3 additional days. The Pluronic P123 was extracted from the filtered solid product with 250 ml ethanol in a Soxhlet extractor for 48h. The particles were characterized in full, as described below.

Measurement of the electroclinic effect (ECE):

The particles were added to toluene at a concentration of 0.05 wt-% and sonicated using a probe sonicator for 30 min (alternating 4 s on and 4 s off) until they were dispersed. Additional toluene then was added to reduce the concentration of particles to 0.005 wt-%. Although a tiny electroclinic effect can be observed in the (chiral) nematic phase⁴², a much larger — by many order of magnitude — ECE occurs in the chiral Smectic-A phase, especially on cooling toward the Smectic-A to Smetic-C phase transition. Thus, for this experiment we have chosen to use the phenyl benzoate liquid crystal (9004, Fig. 1b), which possesses the requisite smectic phases. 9004 was added to the toluene / particle mixture and heated to a temperature T = 115 °C (just below the boiling point of toluene) for several hours to remove the toluene. The procedure resulted in a 0.1 wt-% concentration of particles dispersed in liquid crystal. For the ECE measurements, a cell was constructed using a pair of semitransparent, electrically-conducting indium-tinoxide coated slides that were then coated with the commercial polyamic acid PI-2555 (Dupont). The PI-2555 was imidized by prebaking at 80° for 5 min, followed by a full bake at 250° for 60 min. The slides then were rubbed unidirectionally using a commercial rubbing cloth to create a preferred axis for alignment of the liquid crystal, placed together (separated by Mylar spacers of nominal thickness 6 µm) with the rubbing directions arranged to be antiparallel, and cemented. Two such cells were constructed, one filled by capillary action with 9004 in the isotropic phase, and the other with the 0.1 wt-\% mixture of 9004 and chiral organosilica particles. Each of the cells was placed in an optical setup in which light from a Nd-YaG laser at wavelength 532 nm passed through a polarizer, the cell (where the rubbing direction was at 22.5° with respect to the polarized light), a crossed polarizer, and into a detector. The detector output was input to both a d.c. voltmeter and to a lock-in amplifier, which was referenced to the

driving frequency f = 317 Hz of an a.c. voltage that was applied across the cell. This a.c. voltage was increased in 0.2 V steps with a dwell time of 50 s at each step, and the average induced tilt angle $\theta_{\rm eff}$ of the liquid crystal director, which for this optical geometry⁴⁰ is equal to the a.c. intensity measured by the lock-in amplifier (in amplitude mode) divided by 4 times the d.c. intensity, *i.e.*, $\theta_{eff} = I_{ac}/4I_{dc}$, was recorded.

The Raynes' Geometry experiment:

For the Raynes' geometry experiment⁴¹, two glass microscope substrates were treated with PI-2555 as above, and were arranged with their rubbing directions oriented at 90° with respect to each other. This 90° orientation of the rubbed substrates enforces the boundary conditions described above. The slides were separated by spacer beads of thickness 10 µm, and cemented. Two such cells were fabricated, one filled with pure 5CB liquid crystal (Fig. 1a) and the other with 0.1 wt-% particles. 5CB was chosen for the Raynes' experiment because of its room temperature nematic phase, making it a far more facile material than 9OO4 for this experiment. The samples were imaged using a polarizing optical microscope at room temperature, approximately 23°.

Additional analytical instrumentation:

Solid-state ²⁹Si MAS and ¹³C MAS NMR spectra were recorded with Bruker DRX-500 instrument. Infra-red (IR) spectra were collected by PerkinElmer Spectrum 65 FT-IR spectrometer. Scanning electron microscopy (SEM) and Scanning transmission electron microscopy (STEM) images were acquired by extra high resolution scanning electron microscopy (XHR-SEM) MagellanTM 400L from the FEI company. Images were taken using Shottky-type field emission source with through-lens SE and BSE detector (TLD) and retractable annular BF/DF STEM detectors and scanned at voltages of 20kV and 25kV. Thermogravimetric analysis (TGA) was performed on Mettler Toledo TG 50 analyzer. Measurements were carried out at the temperature range 25–950 °C at a heating rate of 10 °C/min under N₂ atmosphere. Surface area and pore size were determined from N₂ adsorption-desorption isotherms obtained with a NOVA-1200e of Quantachrome instrument, applying the BET and BJH equations.

Results and discussion

Particles characterization:

SEM and TEM images of the sub-micron particles are shown in Fig. 2a, where the convoluted mesopore entrances are clearly seen. Indeed, the shape of the nitrogen adsorption-desorption isotherms (Fig. 2b) and the location of the hysteresis loop are both classical for mesoporisity; the average pore size as calculated from the BET equation is around 9 nm. Consequently, the specific nitrogen-surface area of the chiral particles as determined by the BET equation is 15 m² g⁻¹m²; the excellent agreement with the BET equation (inset of Fig. 2b) is indicative of the homogeneity of the organic-inorganic composite material. The organic-inorganic nature of these particles is reflected in a number of additional analytical methods: The thermal-gravimetric decomposition profile (Fig. 2c) shows a 57 % weight loss centered at 402 °C (following an initial 4 % weight loss centered at 153 °C, representing desorption of physically adsorbed volatile molecules such as water and ethanol), which agrees with the theoretical 70% organics and 30% calculated of SiO_{1.5}, taking into account that the Si-C bonds are converted to Si-O bonds atoms. Solidstate ²⁹Si MAS NMR (Fig. 2d) clearly shows the T³ peak for fully condensed Si and the T² peak for the terminal silanols at -66.33 and -59.02 ppm, respectively. Significantly, no Q peaks appear, since no tetraalkoxysilane precursors were used. The ¹³C MAS NMR spectrum (Fig. 2e) shows, in addition to the aliphatic carbons peaks at 9.44, 14.07, 22.7 and 42.71 ppm, the sugar moiety peaks which appear between 60 and 100 ppm (61.32, 63.53, 71.38, 89.19, 91.71, 94.47, 95.42, 96.74 and 98.74 ppm). Furthermore, the typical carbamate peak is clearly seen at 157.43 ppm. Finally, FT-IR (Fig. 2f) displays the following

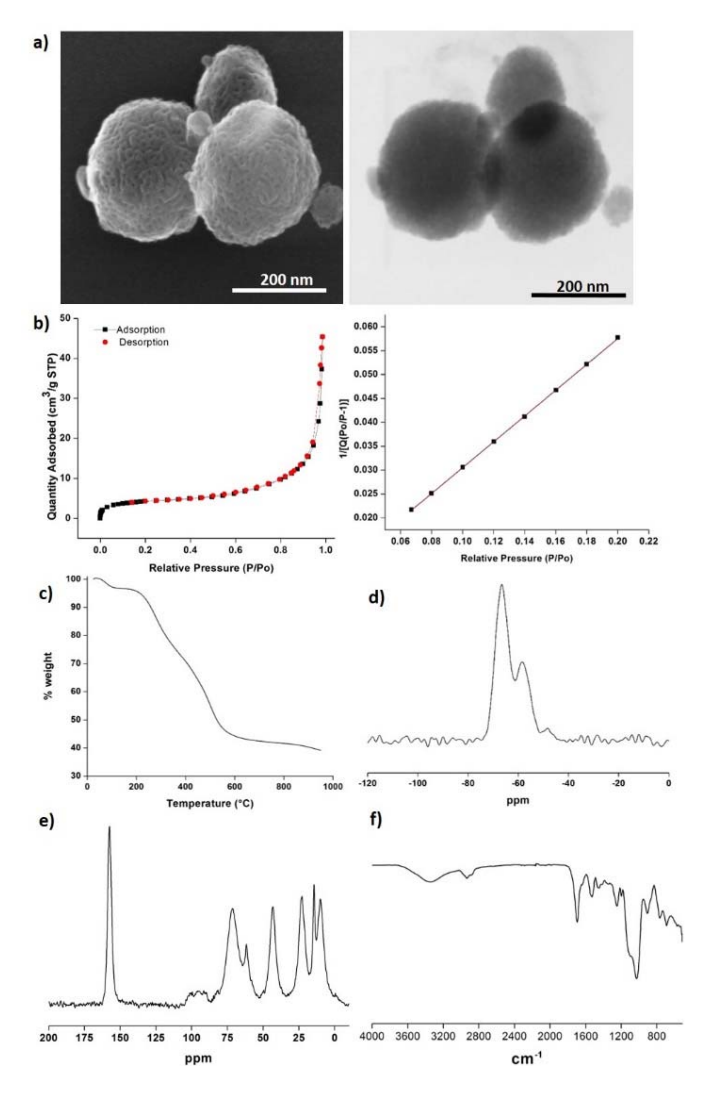


Figure 2 Analyses of the chiral maltose-silica particles: (a) SEM (left) and STEM (right) images of the D-maltose-silica chiral particles. (b) The nitrogen adsorption-desorption isotherms (left) indicating the mesoporosity, and the compliance with the BET equation (right), indicating the homogeneity of the organic-inorganic hybrid material. (c) The TGA profile under nitrogen, indicating the organic-inorganic nature of the composite material. (d) Solid-state ²⁹Si MAS NMR. (e) Solid-state ¹³C MAS NMR. (f) FTIR — see text for interpretation of the peaks in (d), (e) and (f).

indicative peaks: N-H carbamate at 3306 and 1546 cm⁻¹, C=O at 1698 cm⁻¹ and the Si-O-Si wide signal at 1014 cm⁻¹.

The electroclinic chiral effect:

For the ECE measurements, the liquid crystal, 9OO4 (Fig.1b) was used, and we exploited the diverging behavior of the ECE on cooling toward the Sm-A to Smectic-C (Sm-C) phase transition

temperature $T_{AC} \sim 62^\circ$. These measurements were performed for both the particle-doped and the undoped samples as a function of temperature. The results are shown in Figs. 3 and 4. Let us first examine Fig. 3, which shows the effective rotation angle θ_{eff} as a function of the average applied electric field E across the cell. For the undoped 0 wt-% sample, no systematic electroclinic effect was observed, i.e., $d\theta_{eff}/dE \approx 0$, as shown by the black inverted triangles measured close to the transition temperature at $T = T_{AC} + 100$ mK. For the chirally doped 0.1 wt-% sample, θ_{eff} is proportional to E as expected, with the proportionality constant increasing with decreasing temperature toward T_{AC} . Moreover, for temperatures sufficiently far above T_{AC} , mean field theory predicts that the

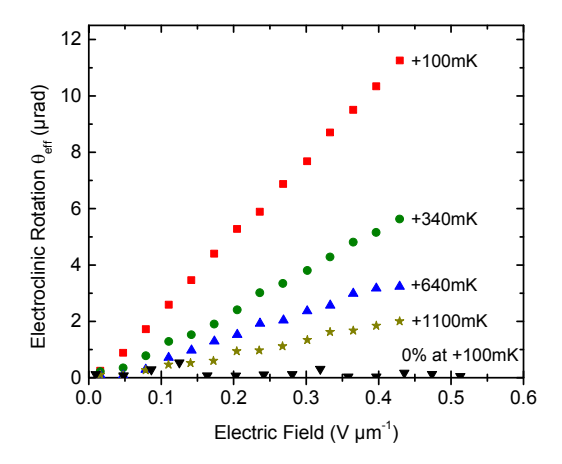


Figure 3 Electroclinic results. The average tilt θ_{eff} is plotted vs. the applied electric field at several temperatures above the Sm-A to Sm-C transition temperature T_{AC} for the chiral doped LC (top four sets of data) and for the undoped achiral LC (the inverted black triangles.)

zero frequency response of $d\theta_{eff}/dE$ should diverge as $1/(T-T_{AC})$ on decreasing temperature in the Sm-A phase³⁸. (Very close to the transition temperature, a critical slowing down of the soft mode occurs. This would cause deviations from $1/(T-T_{AC})$ when the system's response time becomes too slow relative to the driving frequency f very close to T_{AC} . This is not a problem for $T > T_{AC} + 100$ mK in our experiment.) Figure 4 shows data for the slopes $d\theta_{eff}/dE$ collected from two different doped cells at several different positions in each cell. As is apparent, $d\theta_{eff}/dE$ diverges on cooling toward T_{AC} . The

differences in the apparent divergence temperatures is due to small temperature gradients within the cells and spatially-varying concentrations of the particles; this variation becomes more apparent in the inset to Fig. 4, where we plot $(d\theta_{eff}/dE)^{-1}$ vs. temperature. In mean field theory, this quantity should vanish linearly on approaching the transition temperature, which it clearly does.

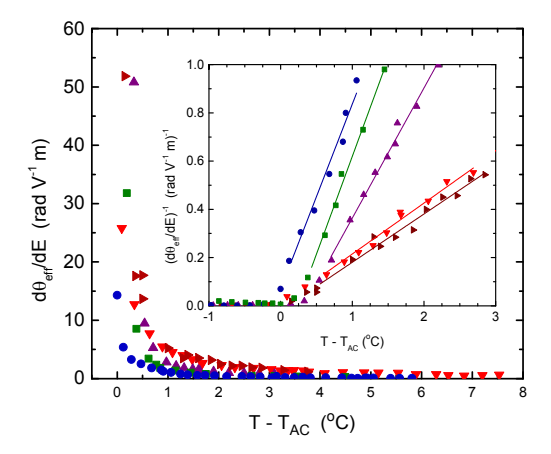


Figure 4 The effective electroclinic coefficients $d\theta_{eff}/dE$ — this corresponds to the slopes of the data in Fig. 3 — vs. temperature above T_{AC} for the chirally doped LC. Data were collected at several points in two separate cells, as described in the text. Inset: The inverse electroclinic coefficient vs. $T - T_{AC}$. As expected from mean field theory, the inverse electroclinic coefficient is approximately linear in T - T_{AC} in the Sm-A phase.

The variation of the slope from one experimental run to the next is due to concentration inhomogeneities and aggregation of the organosilica particles at different positions in the cells. This is a common problem when dealing with suspensions of colloids in liquid crystals. Nevertheless, the clear message from Figs. 3 and 4 is that the undoped sample shows no systematic electroclinic signature that would be characteristic of the chiral Sm-A to Sm-C phase transition, whereas the liquid crystal doped with the chiral organosilica particles exhibits the classic signatures associated with deracemization of the liquid crystal host.

The Raynes' Geometry experiment:

For the Raynes' experiment, Figs. 5a,b are microscope images of the cells, where Fig. 5a shows the nearly straight domain lines without the chiral particles and Fig. 5b shows them in the presence of 0.1

wt-% of the chiral nanoparticles — the evolved curvature lines are clearly seen, where the domain walls terminate at the spacer beads or at other particulates. Note that the orientations of the sample, the polarizer, and the analyzer have been adjusted so that the domain walls are dark and the two domains are of similar hue and brightness. This facilitates a more accurate identification and numerical fitting of the domain boundary. In both images, 15 wall segments were selected and the domain walls were digitized using a Canny algorithm⁴³ to detect and digitize the domain walls. The segments were then numerically fitted to circles to obtain the radii of curvature R, and thus the curvatures C = 1/R. The values of the curvature were averaged, and found to be $C = (0.5 \pm 1.0) \times 10^{-4} \, \mu \text{m}^{-1}$ for the undoped 5CB and $(33 \pm 10) \times 10^{-4} \, \mu \text{m}^{-1}$ for the doped 5CB, clearly indicative of the LC-deracemization effect of the particles. To be sure, this curvature is smaller than would be expected if the particles were to remain fully dispersed; Fig. 5b shows some graininess, which is due to partial aggregation of the particles. Raynes also showed that the helical pitch P of the chiral liquid crystal is equal to 2/C in the equal elastic constant approximation; thus $P = (600 \pm 150) \, \mu \text{m}$ for the chirally doped liquid crystal. This represents an upper limit for P owing to the aggregation seen in Fig. 5b. Finally, note in Fig. 5a that there is a small degree of random wall curvature that occurs on cooling the liquid crystal from the isotropic phase into the nematic phase, which

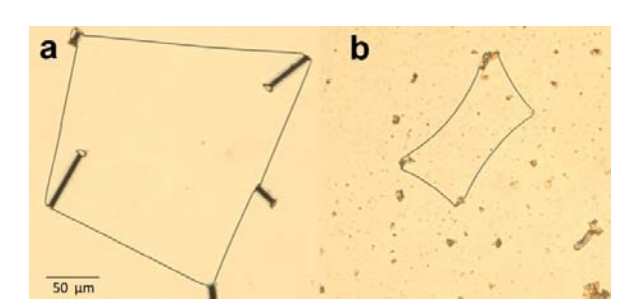


Figure 5 Polarizing micrograph of domain walls. (a) Left: Undoped achiral 5CB. (Heavier line segments are the spacer beads.) (b) Right 0.1 wt-% chiral particles in 5CB, showing domain wall curvature. Note that the enclosed region, which corresponds to the "minority twist", is being squeezed inward by the more energetically favorable twist domain outside. The 50 mm scale bar applies to both (a) and (b).

becomes pinned by a surface memory effect⁴⁴. Nevertheless, the average curvature for the achiral sample is smaller than the experimental variation. The situation is different from the 0.1 wt-% doped sample, where each domain wall clearly is curved, concave inward, toward the minority handedness domain. This is a clear signature of conformational deracemization of the liquid crystal due to the chiral nanoparticles.

Conclusions

Until now chiral organosilica submicron particles for different purposes usually have been prepared by methods other than direct polycondensation of pure trialkoxysilanes. Here, a direct and non-trivial synthesis has been developed and demonstrated using an enantiopure monomer. The resulting chiral maltose organosilica particles were shown to induce conformational deracemization of liquid crystal phases, using two sets of experiments. These two experiments – the electroclinic effect determination and the Raynes experiment, are independent verifications of the chirality of our organosilica particles. These results suggest that this class of organosilica material may be potentially useful for enantiomeric differentiation process such as chromatography and asymmetric catalysis.

Conflicts of interest

There are no conflicts to declare.

Acknowledgements

The authors thank Melvin Santiago for useful discussions. This work was supported by US-Israel Binational Science Foundation, under grant 2014034, the National Science Foundation's Condensed Matter Physics Program under grant DMR-1505389 and the Natural Sciences and Engineering Research Council of Canada.

References

- 1. F. Gelman, D. Avnir, H. Schumann and J. Blum, *Journal of Molecular Catalysis a-Chemical*, 1999, **146**, 123-128.
- 2. A. C. Marr and P. C. Marr, Dalton Transactions, 2011, 40, 20-26.
- 3. P. Kadhirvel, M. Azenha, P. Gomes, A. F. Silva and B. Sellergren, *Journal of Chromatography A*, 2015, **1424**, 59-68.
- 4. H. B. Qiu and S. N. Che, *Chemical Society Reviews*, 2011, **40**, 1259-1268.
- 5. X. W. Wu, J. F. Ruan, T. Ohsuna, O. Terasaki and S. N. Che, *Chemistry of Materials*, 2007, **19**, 1577-1583.
- 6. S. Marx and D. Avnir, Accounts of Chemical Research, 2007, 40, 768-776.
- 7. J. Y. Shi, C. A. Wang, Z. J. Li, Q. Wang, Y. Zhang and W. Wang, *Chemistry-a European Journal*, 2011, **17**, 6206-6213.
- 8. A. Ide, R. Voss, G. Scholz, G. A. Ozin, M. Antonietti and A. Thomas, *Chemistry of Materials*, 2007, **19**, 2649-2657.
- 9. C. E. Song and S. G. Lee, *Chemical Reviews*, 2002, **102**, 3495-3524.
- 10. A. Monge-Marcet, X. Cattoen, D. A. Alonso, C. Najera, M. W. C. Man and R. Pleixats, *Green Chemistry*, 2012, **14**, 1601-1610.
- 11. X. Liu, P. Y. Wang, Y. Yang, P. Wang and Q. H. Yang, *Chemistry-an Asian Journal*, 2010, 5, 1232-1239.
- 12. X. L. Weng, Z. B. Bao, Z. G. Zhang, B. G. Su, H. B. Xing, Q. W. Yang, Y. W. Yang and Q. L. Ren, *Journal of Materials Chemistry B*, 2015, **3**, 620-628.
- 13. D. Herault, G. Cerveau, R. J. P. Corriu and A. Mehdi, *Dalton Transactions*, 2011, 40, 446-451.
- 14. J. Morell, S. Chatterjee, P. J. Klar, D. Mauder, I. Shenderovich, F. Hoffmann and M. Froba, *Chemistry-a European Journal*, 2008, **14**, 5935-5940.

- 15. A. Kuschel, H. Sievers and S. Polarz, *Angewandte Chemie-International Edition*, 2008, **47**, 9513-9517.
- 16. J. J. E. Moreau, L. Vellutini, M. W. C. Man and C. Bied, *Journal of the American Chemical Society*, 2001, **123**, 1509-1510.
- 17. T. Y. Zhuang, J. Y. Shi, C. Ma and W. Wang, *Journal of Materials Chemistry*, 2010, **20**, 6026-6029.
- 18. J. J. E. Moreau, L. Vellutini, M. W. C. Man and C. Bied, *Chemistry-a European Journal*, 2003, **9**, 1594-1599.
- 19. V. Rebbin, R. Schmidt and M. Froba, *Angewandte Chemie-International Edition*, 2006, **45**, 5210-5214.
- 20. G. R. Zhu, H. Zhong, Q. H. Yang and C. Li, *Microporous and Mesoporous Materials*, 2008, **116**, 36-43.
- 21. G. R. Zhu, D. M. Jiang, Q. H. Yang, J. Yang and C. Li, *Journal of Chromatography A*, 2007, **1149**, 219-227.
- 22. I. Sierra, D. Perez-Quintanilla, S. Morante and J. Ganan, *Journal of Chromatography A*, 2014, **1363**, 27-40.
- 23. R. X. Ran, L. J. You, B. Di, W. Q. Hao, M. X. Su, F. Yan and L. L. Huang, *Journal of Separation Science*, 2012, **35**, 1854-1862.
- 24. X. A. Liu, P. Y. Wang, L. Zhang, J. Yang, C. Li and Q. H. Yang, *Chemistry-a European Journal*, 2010, **16**, 12727-12735.
- 25. X. S. Gao, R. Liu, D. C. Zhang, M. Wu, T. Y. Cheng and G. H. Liu, *Chemistry-a European Journal*, 2014, **20**, 1515-1519.
- 26. A. Monge-Marcet, R. Pleixats, X. Cattoen, M. W. C. Man, D. A. Alonso and C. Najera, *New Journal of Chemistry*, 2011, **35**, 2766-2772.

- 27. A. Zamboulis, N. J. Rahier, M. Gehringer, X. Cattoen, G. Niel, C. Bied, J. J. E. Moreau and M. W. C. Man, *Tetrahedron-Asymmetry*, 2009, **20**, 2880-2885.
- 28. A. Brethon, C. Bied, J. J. E. Moreau and M. W. C. Man, *Journal of Sol-Gel Science and Technology*, 2009, **50**, 141-151.
- 29. A. Brethon, P. Hesemann, L. Rejaud, J. J. E. Moreau and M. W. C. Man, *Journal of Organometallic Chemistry*, 2001, **627**, 239-248.
- 30. T. T. Hao, J. Y. Shi, T. Y. Zhuang, W. D. Wang, F. C. Li and W. Wang, *Rsc Advances*, 2012, **2**, 2010-2014.
- 31. R. Basu, K. A. Boccuzzi, S. Ferjani and C. Rosenblatt, *Applied Physics Letters*, 2010, **97**, 121908.
- 32. R. Memmer, H. G. Kuball and A. Schonhofer, *Molecular Physics*, 1996, **89**, 1633-1649.
- 33. R. P. Lemieux, *Chemical Society Reviews*, 2007, **36**, 2033-2045.
- 34. S. Pieraccini, S. Masiero, A. Ferrarini and G. P. Spada, *Chemical Society Reviews*, 2011, **40**, 258-271.
- 35. R. Berardi, H. G. Kuball, R. Memmer and C. Zannoni, *Journal of the Chemical Society-Faraday Transactions*, 1998, **94**, 1229-1234.
- 36. V. Jayalakshmi, T. Wood, R. Basu, J. N. Du, T. Blackburn, C. Rosenblatt, C. M. Crudden and R. P. Lemieux, *Journal of Materials Chemistry*, 2012, **22**, 15255-15261.
- 37. I. R. Nemitz, K. McEleney, C. M. Crudden, R. P. Lemieux, R. G. Petschek and C. Rosenblatt, *Liquid Crystals*, 2016, **43**, 497-504.
- 38. S. Garoff and R. B. Meyer, *Physical Review Letters*, 1977, **38**, 848-851.
- 39. Walba, D.M. and Clark, N.A., "Methods and apparatus for detection of molecular chirality", US Patent 7,374,948 B2 (May 20, 2008).
- 40. G. Andersson, I. Dahl, P. Keller, W. Kuczynski, S. T. Lagerwall, K. Skarp and B. Stebler, *Applied Physics Letters*, 1987, **51**, 640-642.
- 41. E. P. Raynes, *Liquid Crystals*, 2006, **33**, 1215-1218.

- 42. Z. Li, G. A. Dilisi, R. G. Petschek and C. Rosenblatt, *Physical Review A*, 1990, 41, 1997-2004.
- 43. J. Canny, *Ieee Transactions on Pattern Analysis and Machine Intelligence*, 1986, **8**, 679-698.
- 44. N. A. Clark, *Physical Review Letters*, 1985, **55**, 292-295.